Available online at www.sciencedirect.com
ScienceDirect
Ceramics International 34 (2008) 1–6
CERAMICS INTERNATIONAL
www.elsevier.com/locate/ceramint

Electrophoretic deposition and characterization of helical piezoelectric actuator

Y.H. Chen *, T. Li, F.Y.C. Boey, J. Ma

School of Materials Science and Engineering, Nanyang Technological University, Singapore 639798, Singapore

Received 23 January 2006; received in revised form 14 February 2006; accepted 16 July 2006
Available online 12 September 2006

Abstract

The helical actuator was successfully fabricated using the versatile technique of electrophoretic deposition (EPD), which was achieved by depositing two electrode-separated layers of PZT powders on the helical shaped substrate and co-sintering. The actuator is able to generate a rotational displacement Δl in the circumferential direction and also a radial displacement ΔR in the radial direction, as a result of field-induced rotation of the cross section. Theoretical analysis and experimental results show that the displacements are linearly proportional to the number of the turns n and applied electric field. And also, rotational motion shows larger displacement than the radial motion due to the circular configuration. For the fabricated actuator (45.76 mm in length, 4.09 mm in outer diameter, 0.55 mm in the wall thickness and 4 turns), approximately 43 and 9 μm displacements have been achieved for the rotational and radial motions, respectively.

Keywords: A. EPD; B. Helical; C. Piezoelectric; E. Actuator

1. Introduction

Large stroke and generative force are always the primary but challenging requirements for the piezoelectric actuators. The normal soft and hard PZT materials are only able to produce a strain less than ~0.2% [1,2]. Even using the high strain single crystal or piezoelectric polymers, the strain is also limited by ~1% [1,2] and ~5% [3], respectively. As a result, to improve the actuation performance of the device, various amplification mechanisms and approaches have been proposed and applied. These mechanisms include the internal and external leveraging [1]. Examples are multilayer stacks and benders for the internal leveraging mechanism; and lever arm and hydraulic amplification for the external leveraging mechanism.

In the recent years, an internally leveraged helical piezoelectric actuator has been reported, which generates large static rotational displacement up to several degrees [4]. The super-helix formed by the wound helical actuator can even amplify the strain to linear displacement up to millimeters [5], which makes the actuator promising in the application in camera auto-focusing systems. However, the manufacturing of the actuator is quite difficult. This is the reason that the theoretical design of the actuator has existed for many years, however, the device was only achieved in the recent years [5]. An approach of green ceramic tape lamination process followed by plastic deformation has been reported to fabricate the helical actuator [4]. The method follows the procedures: preparing the ceramic tape by extrusion, screen printing the electrode, sticking the two tapes by pressure rolling, winding the tape to the machined former and final co-sintering.

This procedure is quite difficult, complex and expensive. Hence, this paper proposes another more effective approach – electrophoretic deposition (EPD) – to form the helical actuator. EPD is a colloidal process wherein ceramic bodies are shaped directly from a stable colloid suspension by a dc electric field. It has been proven to be a simple method to form the complex shapes with low cost [6-8]. Using this technique, both the thin film and bulk ceramics can easily be formed, such as multilayers, tubes and fibers [9–11]. However, such a complex shape – helix – was not found to be achieved using EPD in the literature. In this paper, we introduce the procedures to fabricate the helical actuator using EPD. The formed actuator was also characterized and theoretically analyzed in electromechanical properties.

2. Theoretical analysis

Fig. 1 shows the structure and working principle of the helical actuator. It consists of the outer electrode, inner

* Corresponding author. Tel.: +65 63168930; fax: +65 67909081.
E-mail address: chenyh@ntu.edu.sg (Y.H. Chen).

0272-8842/$32.00
doi:10.1016/j.ceramint.2006.07.009

electrode, intermediate electrode and the PZT layers between them as shown in Fig. 1(a). The PZT materials can be either parallelly poled or antiparallelly poled. The whole actuator shows a helical shape. From the configuration of the actuator, it can be regarded that the helical actuator is essentially a helical shaped bimorph actuator.

Finite element analysis (FEA) using ANSYS as shown in Fig. 1(b) indicates that under clamped-free boundary conditions, when driving voltage is applied to the actuator, due to the well-known bending motion in the bimorph and helical shape of the whole structure, the cross section of the actuator rotates and the free tip of the actuator will move along the circumferential direction. For example, the free tip will travel from the original location A to the final location B, as a result, producing a rotational displacement Δl. Meanwhile, the radius of the helical actuator will change ΔR as shown in the figure.

To quantificationally describe the motion of the helical actuator, Δl and ΔR are derived in the following manner. It is assumed that the displacement is the stack of n bimorph circles. Each circle produces the same displacement. The derivation starts from the standard theories of strength of materials and piezoelectric ceramics. For the bimorph actuator, it has been known that the normal stress in the location above and below the neutral plane can be expressed as [12]

$$T_1 = YS_1 \pm Yd_{31}E_3 \tag{1}$$

where T_1 is the stress, S_1 the strain, Y the Young's modulus, d_{31} the piezoelectric constant and E_3 is the electric field. For a curved beam, the neutral plane usually does not coincide with the center of the beam. If the cross section is a rectangle, the radius of curvature of the neutral plane r has the following expression [13]

$$r = \frac{2h}{\ln R_1/R_2} \tag{2}$$

where h is the thickness of a single layer of PZT ceramic plate and R_1 and R_2 are the outer and inner radii of the actuator, respectively. The strain S_1 in Eq. (1) can be written as [13]

$$S_1 = \frac{z}{r+z}\frac{\mathrm{d}\theta}{\mathrm{d}\varphi} \tag{3}$$

where z is the distance from the neutral plane. And $\mathrm{d}\theta/\mathrm{d}\varphi$ stands for the angle of rotation of a cross section at angle φ. φ starts from 0 at the clamped end to $2n\pi$ at the free end of the actuator.

The plane torque at an arbitrary cross section is the integration of the product of T_1 and z over the whole cross section area A

$$M = \int_A T_1 z\,\mathrm{dA} = 0 \tag{4}$$

Because there is no external load, M is zero [14]. Therefore, applying Eqs. (1)–(3) into (4), and from the solutions, it is found that

$$\frac{\mathrm{d}\theta}{\mathrm{d}\varphi} = d_{31}E_3\frac{(1/2)[(R_1-r)^2+(R_2-r)^2]}{(1/2)(R_1^2-R_2^2)-(R_1-R_2)^2/(\ln R_1/R_2)} \tag{5}$$

For helical actuator with n turns, the total angle of rotation $\Delta\theta$ can then be obtained by integrating φ from 0 to $2n\pi$. Therefore,

$$\Delta\theta = 2n\pi d_{31}E_3\frac{(1/2)[(R_1-r)^2+(R_2-r)^2]}{(1/2)(R_1^2-R_2^2)-(R_1-R_2)^2/(\ln R_1/R_2)} \tag{6}$$

The angle of rotation $\Delta\theta$ also indicates that the displacement Δl along the circumferential direction travels an amount of $r\Delta\theta$, i.e.,

$$\Delta l = 2n\pi d_{31}E_3\frac{(r/2)[(R_1-r)^2+(R_2-r)^2]}{(1/2)(R_1^2-R_2^2)-(R_1-R_2)^2/(\ln R_1/R_2)} \tag{7}$$

Δl is approximately the change of the perimeter. This will induce a radial displacement ΔR. Because the perimeter change Δl can also be expressed as $2\pi(R_{\text{original}} - R_{\text{final}})$ (i.e., $2\pi\Delta R$), the radial displacement ΔR is then obtained as

$$\Delta R = nd_{31}E_3\frac{(r/2)[(R_1-r)^2+(R_2-r)^2]}{(1/2)(R_1^2-R_2^2)-(R_1-R_2)^2/(\ln R_1/R_2)} \tag{8}$$

The above-derived equations indicate that Δl and ΔR are proportional to the piezoelectric constant, electric field, number of turns and also affected by radii of the actuator.

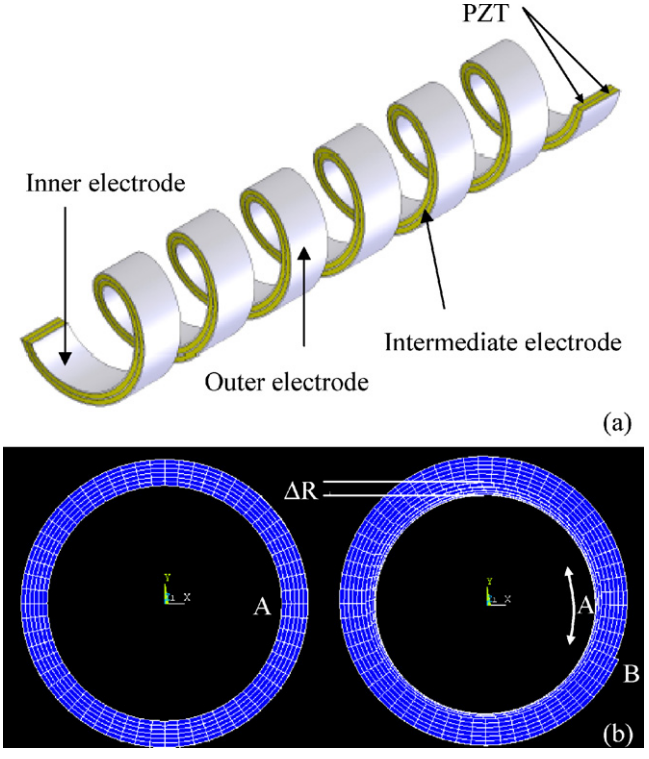

Fig. 1. (a and b) Structure and working principle of the helical actuator.

3. Fabrication procedure

To fabricate the helical actuator, a doped piezoelectric PZT powder, $0.95Pb(Zr_{0.52}Ti_{0.48})O_3{\cdot}0.03BiFeO_3$ $\cdot 0.02Ba(Cu_{0.5-}$

$_{0.5})O_3$ + 0.5wt%MnO_2 [15–17] was used as the starting material. In this material, both $BiFeO_3$ and $Ba(Cu_{0.5}W_{0.5})O_3$ act as sintering additives and form a solid solution with $Pb(Zr,Ti)O_3$ to result in a complex perovskite-type phase. The sintering additives reduce the chance of crack generation and distortion of the actuator during sintering. The small amount of MnO_2 was added to improve the hardness of the piezoelectric ceramics. This powder was prepared using conventional oxide mixing method. The raw oxide powders were mixed and horizontally ball-milled for 24 h to increase the homogeneity. Then, it was calcined at 750 °C for 2 h before planetary ball-milling at 150 rpm for 8 h.

The suspension for EPD was prepared by adding the PZT powder in ethanol with the concentration of 50 g/l. Ten percent HNO_3 was applied to adjust the pH of the suspension. The suspension was stirred for 6 h to make sure the complete dispersion of the powders in the medium. The characteristics of the suspension have been shown in Fig. 2. It can be seen that the particle size distributes within the range of 0.8–1.3 μm. The average particle is around 1 μm. A narrow particle size distribution is usually expected because it helps to form a uniform structure during the electrophoretic deposition [18]. A pH between 4 and 5 is noted to be optimum since the zeta potential is maximum in this range. Zeta potential is an indicator of the stability of the suspension [19]. A high absolute zeta potential represents a well dispersed and stable suspension. Hence in the following deposition, the suspension pH was controlled to be 4.6.

The electrophoretic deposition system is schematically shown in Fig. 3. The electrophoretic cell includes a graphite rod substrate as the cathode and a stainless steel as the anode. During deposition, the charged PZT particles move towards and deposit on the cathode. The graphite substrate was machined into a helical shape as shown in Fig. 4(a). The substrate was immersed into the suspension and the deposition was performed for 4 min under a constant applied dc voltage 50 V. After that, the deposits were dried for 12 h and coated with a layer of platinum conductive paste. After drying of the paste, the second deposition was conducted for 5.5 min at 60 V.

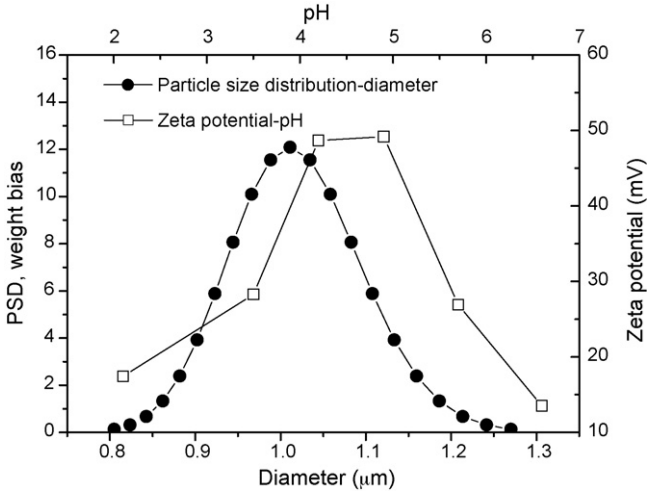

Fig. 2. Characteristics of the suspension.

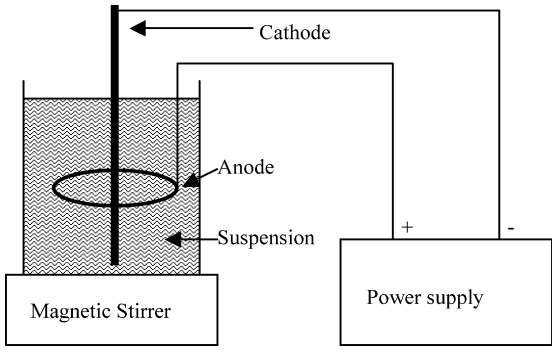

Fig. 3. Setup for electrophoretic deposition system.

The increase of deposition duration and voltage is mainly due to the less conductivity of the platinum paste before densification. The deposits were also completely dried in a dry keeper for 12 h. The deposits were then fired at 600 °C for 1 h to burn out the graphite rod substrate. Fig. 4(b) shows the product after this stage. It was then sintered at 1100 °C for 1 h. Fig. 4(c) shows the products after sintering. The insert of Fig. 4(c) shows a piece of cross section of the product. The platinum electrode can be clearly seen and is about 7 μm. The density of the whole structure is 7.6 g/cm^3, 96% of the theoretical density of the PZT materials. Finally, the sintered deposits were coated with silver paste and densified at 800 °C for 20 mins. Poling was carried out in silicone oil at 100 °C for 30 mins under 2 kV/mm. The finally obtained actuators are shown in Fig. 4(d). Varying the dimension and pitch of the graphite rod substrate, more dimensional helical actuators are available based on the above method.

4. Characterization of electromechanical properties

The displacement of the fabricated helical actuators was measured using a system consisting of a RT6000HVS ferroelectric tester (Radiant Technologies, Inc.), a Vibraplane (RS Kinetic Systems, Inc.) and a MTI-2000 fotonic sensor (MTI Instruments) as shown in Fig. 5(a). One end of the actuator was clamped to the vibraplane. The other end remained the free state. A triangle signal at 2.5 Hz was applied to the actuator via the ferroelectric tester. The field-induced displacement was measured using the fotonic sensor. Both the rotational displacement Δl and the radial displacement ΔR were measured. To examine the effect of number of turns n, Δl and ΔR at various locations indicated by the arrows in Fig. 5(b) was measured as a function of applied voltages.

The measured helical actuator has a dimension of 45.76 mm in length, 4.09 mm in outer diameter, 0.55 mm in the wall thickness and 4 turns. Fig. 6 shows the measured results. Fig. 6(a) is the field-induced displacement hysteresis loop of the rotational motion Δl and radial motion ΔR at the 4th turn and applied voltage 100 V. Due to the presence of the electro-mechanical loss, there is displacement hysteresis between the increasing and decreasing direction of the applied voltage [20]. The radial motion shows smaller hysteresis due to the smaller displacement in the corresponding direction. This may also

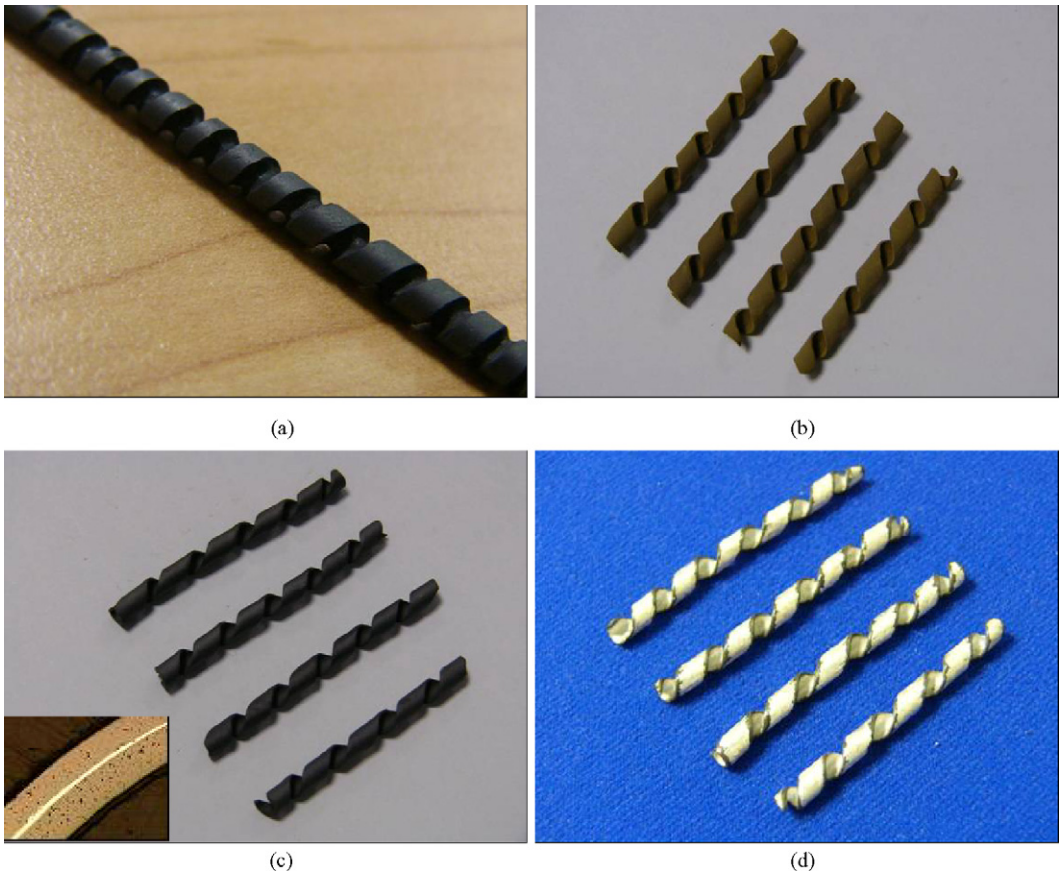

Fig. 4. Photographs of the samples: (a) graphite rod, (b) the deposits after burning out the graphite rod, (c) the deposits after sintering and (d) the deposits after poling.

indicate hysteresis and losses are amplitude dependent. It is also noted that the rotational motion is approximately 43 μm at 100 V, much larger than the radial motion of 9 μm. This is consistent with the theoretical analysis derived earlier. However, it is expected that the rotational motion is 2π times that of the radial motion. The discrepancy may be caused by the neglect of the pitch of the helix during modeling. And also after deformation, the shape of the actuator will deviate from a perfect circle. Fig. 6(b and c) shows the variation of displacement Δl and ΔR as a function of applied voltage at

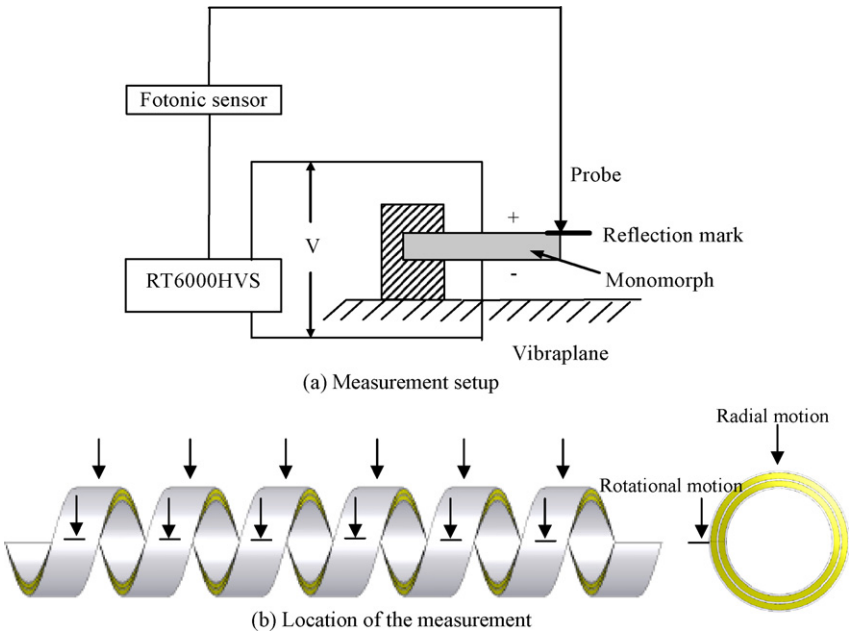

Fig. 5. (a and b) Setup for displacement measurement.

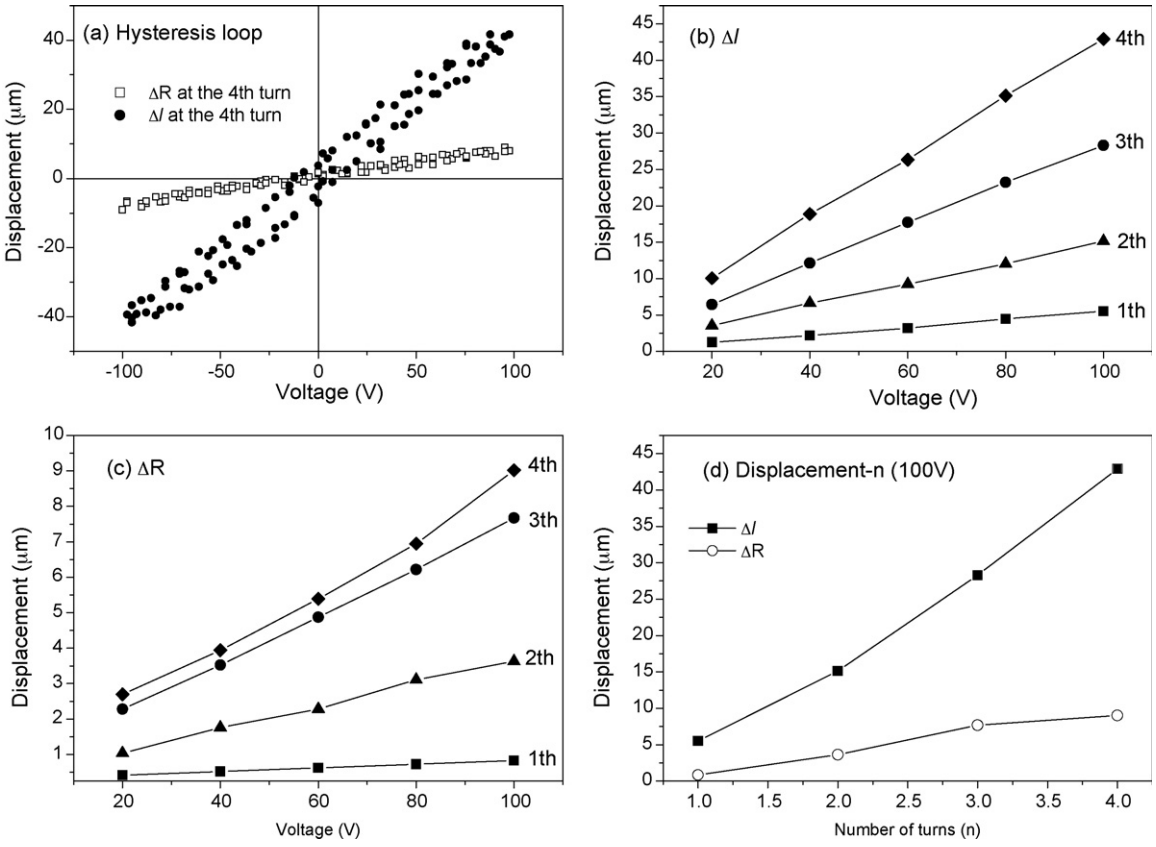

Fig. 6. (a–d) Electric field induced displacement of the helical actuator.

various turns. It can be found that the displacement increases linearly with the increase of the applied voltage. This result also agrees well with the theoretical derivation. Fig. 6(d) shows the relationship between displacement and number of turns n at 100 V. The expected linear relationship has been observed. Therefore, from Fig. 6, it can be concluded that both Δl and ΔR increase linearly with the applied voltage and number of turns.

5. Conclusions

The helical actuator was fabricated successfully using EPD technique, which shows the ability of EPD in processing of the complex shaped ceramic devices. The helical actuator produces both rotational and radial displacement due to the rotation of cross section under the applied electric field. Both displacements are linearly proportional to the number of turns and applied electric field. However, the rotational motion is larger than the radial motion. For the actuator with a dimension 45.76 mm in length, 4.09 mm in outer diameter, 0.55 mm in the wall thickness and 4 turns, approximately 43 μm of rotational displacement and 9 μm of radial displacement have been achieved, respectively.

References

[1] C. Niezrecki, D. Brei, A. Moskalik, Piezoelectric actuation: state of the art, Shock Vibr. Digest 33 (4) (2001) 269–280.
[2] S.E. Park, T.R. Shrout, Ultrahigh strain and piezoelectric behavior in relaxor based ferroelectric single crystal, J. Appl. Phys. 82 (1997) 1804–1811.
[3] A. Strachan, W.A. Goddard III, Large electrostrictive strain at gigahertz frequencies in a polymer nanoactuator: computational device design, Appl. Phys. Lett. 82 (2005), 83103-1-3.
[4] D.H. Pearce, K.A. Seffen, T.W. Button, Net shape formed spiral and helical piezoelectric actuators, J. Mater. Sci. 37 (2002) 3117–3122.
[5] D.H. Pearce, A. Hooley, T.W. Button, On piezoelectric super-helix actuators, Sens. Actuators, A 100 (2002) 281–286.
[6] M. Nagai, Y. Yamashita, Y. Takuma, Electrophoretic deposition of ferroelectric barium titanate thick films and their dielectric properties, J. Am. Ceram. Soc. 76 (1993) 253–255.
[7] B. Ferrari, R. Moreno, Electrophoretic deposition of aqueous alumina slips, J. Eur. Ceram. Soc. 17 (1997) 549–556.
[8] P. Sarkar, X. Huang, P.S. Nicholson, Structural ceramic microlaminates by electrophoretic deposition, J. Am. Ceram. Soc. 75 (1992) 2907–2909.
[9] P. Sarkar, O. Prakash, P.S. Nicholson, Micro-laminate ceramic composites (YSZ/Al_2O_3) by electrophoretic deposition, Ceram. Eng. Sci. Proc. 15 (1994) 1019–1027.
[10] F. Harbach, H. Neinburg, Homogeneous functional ceramic components through electrophoretic deposition from stable colloidal suspensions-I. Basic concepts and application to zirconia, J. Eur. Ceram. Soc. 18 (1998) 675–683.
[11] I. Zhitoirsky, L. Gal-Or, Formation of hollow fibers by electrophoretic deposition, Mater. Lett. 38 (1999) 10–17.
[12] J.V. Randeraat, R.E. Setterington, Piezoelectric Ceramics, Mullard Limited, London, 1974.
[13] W.A. Nash, Strength of Materials, third ed., McGraw-Hill, Inc., 1994.
[14] K. Yao, W.G. Zhu, L.C. Lim, Design and fabrication of a high performance multilayer piezoelectric actuator with bending deformation, IEEE Trans. Ultrason. Ferroelectr. Freq. Control 46 (1999) 1020–1026.

[15] J.F. Li, S.N. Wang, R. Watanabe, Properties of modified lead zirconate titanate ceramics prepared at low temperature (800 °C) by hot isostatic pressing, J. Am. Ceram. Soc. 83 (2000) 955–957.
[16] S. Kaneko, D. Dong, K. Murakami, Effect of simultaneous addition of $BiFeO_3$ and $Ba(Cu_{0.5}W_{0.5})O_3$ on lowering of sintering temperature of $Pb(Zr, Ti)O_3$ ceramics, J. Am. Ceram. Soc. 81 (1998) 1013–1018.
[17] D.Z. Dong, K. Murakami, S. kaneko, Behavior of morphotropic phase boundary in low-temperature sintered lead zirconate–titanate ceramics with $BiFeO_3$ and $Ba(Cu_{0.5}W_{0.5})O_3$, Jpn. J. Appl. Phys. 33 (1994) 5529–5532.
[18] S. Sugiyama, A. Takagi, K. Tszuk, $(Pb,La)(Zr,Ti)O_3$ films by multiple electrophoretic deposition/sintering processing, Jpn. J. Appl. Phys. 30 (1991) 2170–2173.
[19] O.O.V.D. Biest, L.J. Vandeperre, Electrophoretic deposition of materials, Annu. Rev. Mater. Sci. 29 (1999) 327–352.
[20] K. Uchino, S. Hirose, Loss mechanisms in piezoelectrics: how to measure different losses separately, IEEE Trans. Ultrason. Ferroelectr. Freq. Control 48 (2001) 307–321.